Volume 304 • Number 10 • October 2019 www.mme-journal.de

Macromolecular Materials and Engineering

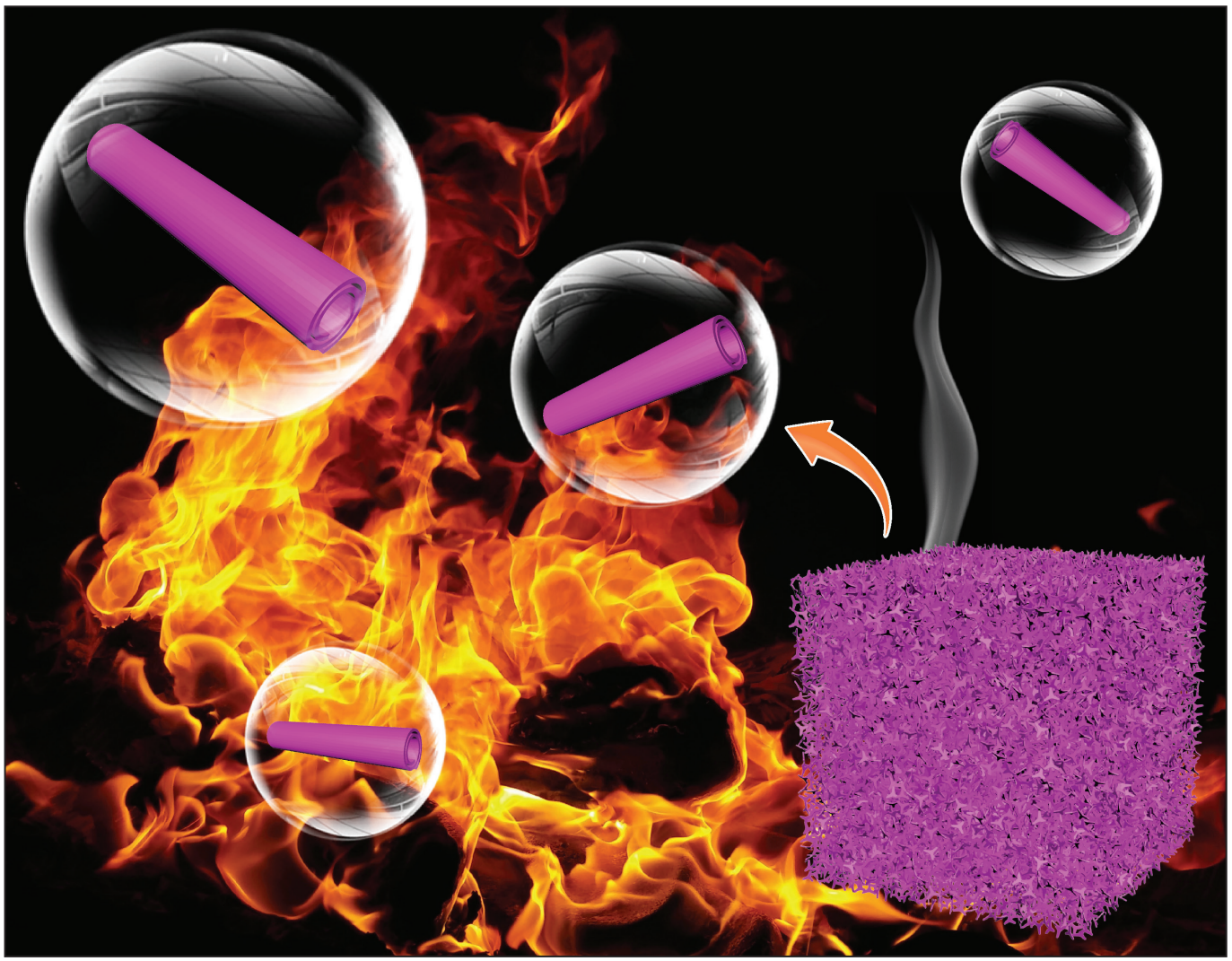

10/2019

WILEY-VCH

Macromolecular Materials and Engineering
www.mme-journal.de

Two in One: Modified Polyurethane Foams by Dip-Coating of Halloysite Nanotubes with Acceptable Flame Retardancy and Absorbency

*Fan Wu, Jingqi Zheng, Xianfeng Ou, and Mingxian Liu**

Poor flame retardancy of polyurethane foam (PUF) limits its practical application in many fields. Here, flame-retardant performance of PUF is improved by a simple dip-coating method. Halloysite nanotube (HNT) coating can be uniformly bonded to PUF surfaces via hydrogen-bonding interactions, which is confirmed by element mapping and X-ray photoelectron spectra. Density and mechanical properties of PUF increase with the concentration of HNT suspension, while porosity of the foam decreases with HNT loading. Weight ratio of HNTs to PUF in the composite can be achieved as high as 65.2%. Surfaces of PUF transfer from hydrophobic to super-hydrophilic after HNT coating, and the water contact angle decreases from 116° to 0° after HNT coating. As a result, methylene blue adsorption capacity of HNTs-coated PUF increases from 0.02 to 0.15 mg g^{-1}, and adsorption efficiency can reach 98% after 10 s. HNT coating can prevent PUF from burning and dripping, which suggests that flame-retardant performance of PUF is significantly improved by HNTs. This work establishes a general procedure for improving flame retardancy and dye absorbency of polymer materials by simple dip-coating of environmental-friendly clay nanotubes, which shows great potential in high-performance polymer and functional composite materials.

1. Introduction

Polyurethane (PU) is the sixth-largest polymer with an annual production of about 17.565 million tons in the world.[1] Various PU products in the form of fiber, film, foam, and bulk material are used in many fields, and mechanical properties of PU can be tailored by changing the material composition and fabrication condition.[2] Among them, polyurethane foam (PUF) is the most used PU product, which is widely used in modern home decoration in soft furniture.[3,4] Generally, PUF has merits including low density, high adsorption, good air permeability, low compression deformation, resistance to organic solvents, ventilation, sound insulation, and heat preservation.[5–7] The common application of PUF is filling materials in furniture mats, vehicle seat mats, and various soft padded laminate composite.[8] However, PUF is easy to burn and its combustion process is very fast.[3,9,10] Because of open-cell structure of PUF, contact area with air is relatively large during combustion. PUF is prone to be ignited and flame easily spreads without self-extinguishment.[11] Therefore, it is of great practical significance to improve flame-retardant performance of PUF.

To improve fire resistance of PUF, doping with flame retardants containing halogen, nitrogen, and phosphorus compounds by mechanical mixing, or chemically linking of flame retardants into molecular chains of PU are usually adopted.[12–14] However, PUF with these flame retardants may release large amounts of toxic gases during combustion (e.g., CO, HCN, dioxins).[15–17] There is an increasing trend in searching for environmental-friendly and sustainable flame retardants. Sol-gel technique and layer-by-layer (LbL) assembly technique can introduce coatings onto the surfaces of PUF, while they do not affect the foam manufacturing process and exhibit a good flame retardancy.[6,12,18] For example, a multilayer film is deposited on PUF by LbL assembly method using cationic chitosan and anionic sodium alginate as raw materials. The composite coating significantly improves the char formation during combustion.[19] LbL assembly of chitosan/poly(allylamine diphosphonate) coating reduces flammability of open-cell PUF.[20] However, most of these coating techniques depend on tedious conditions and require special skills, so it is difficult to meet practical requirements.[21] Nanoparticles including clay and carbon nanotubes significantly improve flame retardancy of PUF via LbL coating process.[22]

Moreover, nanoparticle-coated PUF exhibits improved mechanical properties.[23–25] Using montmorillonite and graphene as raw materials, the composite of PUF shows good physical barrier effect.[26] The reduced flammability is primarily attributed to the formation of an insulating carbonaceous char barrier which reduces heat release rate and mass/energy transfer during combustion.[27,28] However, effective assembling nanoparticles on PUF surfaces and improving the stability of the coating is challenging.

F. Wu, J. Zheng, X. Ou, Prof. M. Liu
Department of Materials Science and Engineering
Jinan University
Guangzhou 510632, P. R. China
E-mail: liumx@jnu.edu.cn

The ORCID identification number(s) for the author(s) of this article can be found under https://doi.org/10.1002/mame.201900213.

DOI: 10.1002/mame.201900213

In recent years, as a natural 1D nanomaterial with abundant resources, halloysite nanotubes (HNTs) have attracted a lot of attention in the application of functional materials.[29] HNTs come from natural silicate clay mineral, which exists mainly in the form of nanotubes. The chemical formula of halloysite is $Al_2Si_2O_5(OH)_4 \cdot nH_2O$, which consists of multiplexed rolled kaolinite sheets of octahedral gibbsite $Al(OH)_3$ and tetrahedral SiO_4. The different layers are interconnected by hydrogen bonds formed between the oxygen atoms of the tetrahedral sheet and the inner surface.[30,31] The inner diameter of tubes is in the range of 10–20 nm and the length ranges from 200 to 1000 nm, which gives a high aspect ratio. Moreover, since the interactions between the tubes are weak, HNTs can be more easily dispersed in solvent and polymer matrix by stirring or sonication process.[32] HNTs have many advantages including large surface area, high aspect ratio, high thermal stability, good mechanical properties, rich pore structures, and sufficient hydroxyl groups, which make them suitable for a variety of composite applications.[33] For example, HNTs coating on 3D printed polylactic acid pattern surfaces effectively enhances interactions with cells and induces orientation growth of stem cells.[34] Literature has shown that HNTs exhibit excellent potentials in improving thermal stability and reducing flammability of polymers.[35–37] Hydroxyl groups of HNTs during combustion occur condensation to produce water in the temperature range of 400–500 °C, which is one of reasons for improving flame retardancy of polymers. Recently, flame-retardant PUF has been obtained composed with HNTs and branched polyethyleneimine or poly(acrylic acid) by LbL assembly method.[38] However, the LbL technique is very complicated and time-consuming, which limits their practical applications.

In this work, we have developed a method for manufacture of flame-retardant PUF by coating of HNTs via a simple dip-coating method. Time for the coating process can be as less as 30 s. Mechanical properties, hydrophilicity, thermal stability, and fire resistance of PUF are significantly improved and can be tailored by the concentration of HNTs suspension. For this method, no dispersant or polymer is added in HNTs suspension formulation. This provides an environmental-friendly alternative to combustible polymer foams with required mechanical flame retardancy, which can be extended to other polymer foams or fibers. Moreover, dye removal ability of PUF is significantly improved by coating of HNTs layer. This work opens up a novel route to fabricate functional polymer materials by a simple way using environmental-friendly and low-cost natural nanoparticles, which shows several advantages such as simple, effective, cheap, and diverse.

2. Results and Discussion

2.1. Structure of HNTs Coated PUF (HNTs-PUF)

Due to hydrophilicity, small size, and high surface charge of HNTs, the nanotubes can be easily dispersed in water by mechanical stirring or ultrasonic treatment.[39,40] Raw HNTs show typical tubular structure with empty lumen morphology and wide size distribution. The size of raw HNTs ranges from 92.6 to 900.9 nm with average size of 389.0 nm (Figures S1 and S2, Supporting Information). The HNTs possess a negatively charged surface with a zeta potential of −22.1 mV. In order to improve flame retardancy of PUF, a layer of HNTs was assembled on the surfaces of PUF by a facile dip-coating method. **Figure 1**B shows digital photographs of PUF and HNTs-PUF. HNTs are uniformly distributed on the surfaces of PUF, and color of HNTs-PUF becomes slightly darker as increases in the suspension concentration. This can be understood by that the surfaces of PUF coated with HNT layers cause original color to be partly covered. This suggests that HNT suspension is evenly dispersed after ultrasonication treatment, and repeated turning during drying process can result in uniform HNT coating on PUF surfaces. It should be pointed out that squeezing the foam during the immersing process is necessary in order to allow HNT suspension to enter inner space of the foam.

Microstructure of HNTs-PUF was then characterized by polarized optical microscope (POM) and scanning electron microscope (SEM). The anisotropic nanoparticle with a certain concentration can form liquid crystal phase in water or polymer solution.[41] Previous studies show that self-assembled liquid crystal phase and gel behavior can be achieved by mixing HNTs and water.[42] The formation of liquid crystal of nanoparticles is beneficial for their assembly on polymer surfaces since it is more stable without aggregates.[43] Figure 1C shows POM images of PUF and modified PUF under white light and polarized light. The PUF has a porous network skeleton with smooth fiber surfaces. In contrast, a layer of HNTs is coated on the porous network skeleton of the PUF without obvious agglomerates and most of cells remain opened. The coating of HNTs does not damage original structure and morphology of PUF. Both foams exhibit an inherent 3D interconnected network and a highly porous structure with the pore diameter of 200–500 μm. Interestingly, a very thin HNT film similar to optical birefringence of liquid crystal phase is formed on some of pore walls of PUF skeleton. As the HNT content increases, the phenomenon of birefringence also becomes stronger.

Difference in the rotation angle of the PUF sample also causes the birefringence phenomenon to change (Figure S3, Supporting Information). This may be because the phenomenon of birefringence is related to the oriented alignment of nanotubes during self-assembly. The structure is preserved in the final stage after water droplet evaporation. The formation of the film in a pore is related to small dimension of the pore and the surface tension of HNTs aqueous suspension, which is like the toy of blowing bubbles using soap water.

Microstructure of PUF and HNTs-PUF was further observed by SEM (**Figure 2**). It is clear that the pore wall of PUF is relatively clean and smooth. Consistent with previous observations, when concentration of HNT suspension increases, more nanotubes exist on PUF skeleton. It can also be seen that surfaces of PUF with different HNT content are rougher and uniformly covered with a layer of nanotubes. Meanwhile, the number of opened cells of PUF decrease slightly as the concentration of HNTs increases since HNTs can block some pores, especially at high concentration. However, the treated PUF still maintains a porous structure which will be shown in the following results. This suggests that HNT coating cannot harm the foam properties related to porous structure of PUF such as heat insulation and sound absorbing.

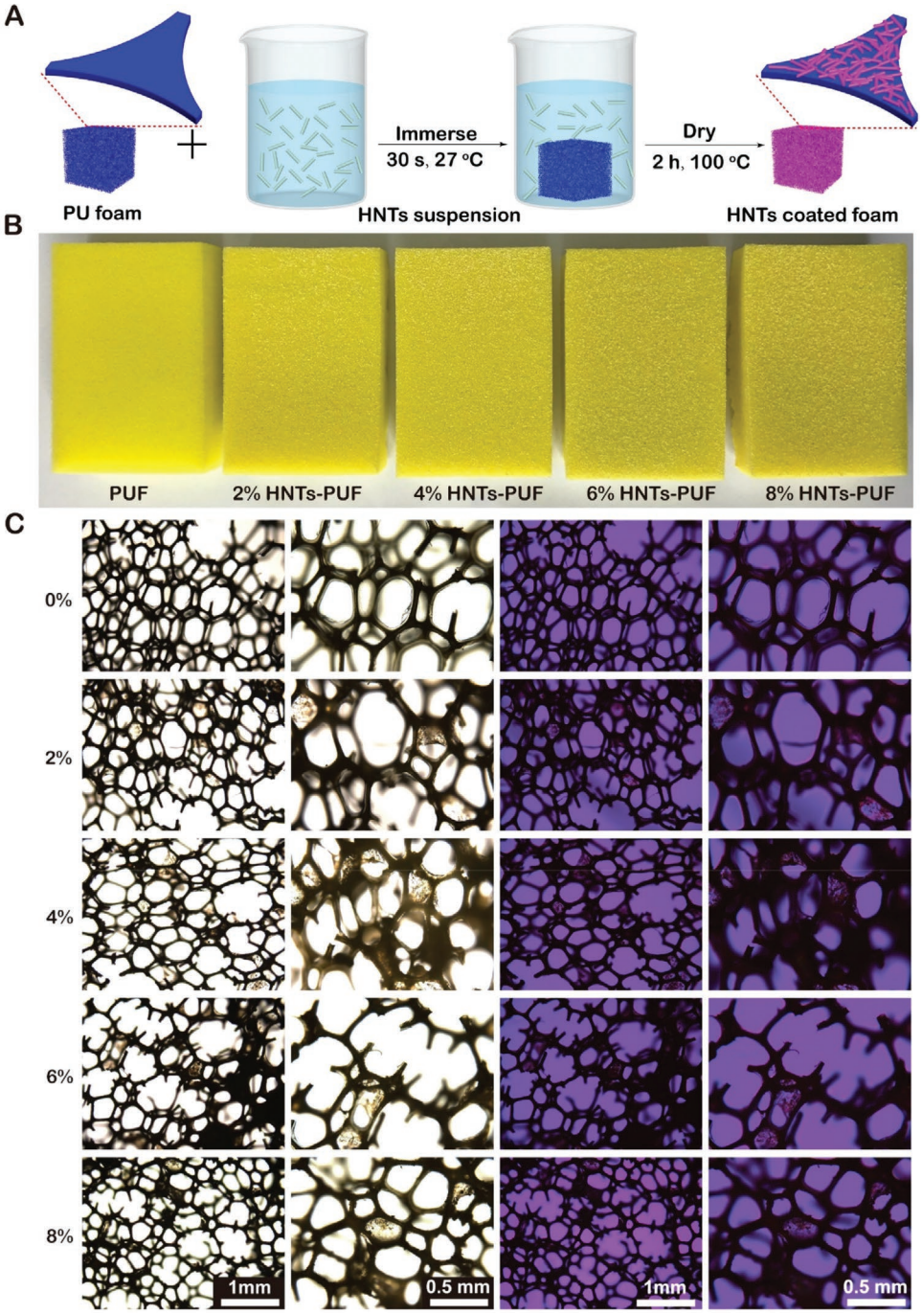

Figure 1. A) Schematic diagram of the preparation process of HNTs-PUF via dip-coating method. B) Digital photographs of PUF and HNTs-PUF (size: $95 \times 65 \times 22$ cm^3). C) POM images of PUF and HNTs-PUF in different magnifications (the left two columns: white light; the right two columns: polarized light with addition of the sensitive tint plate insertion).

2.2. Composition of HNTs-PUF

The surface topographies of pore wall before and after HNT coating were characterized by high-magnification SEM images (**Figure 3**A). HNTs are uniformly distributed in an arbitrary arrangement on the surfaces of PUF skeleton, and original structure of PUF pore is not destroyed during the coating process. Moreover, the surfaces of PUF are not completely smooth, which facilitates the fixation of HNTs on their surfaces. Due to the possible hydrogen bonding interactions between HNTs and PUF, HNT coating can be firmly bonded to the surfaces of PUF. To further demonstrate the successful introduction of HNTs on PUF surfaces, an X-ray photoelectron spectrum (XPS) scan of the untreated and treated PUF surface is performed (Figure 3B,C). A significant difference between the elemental composition of the PUF is found before and after HNT coating. HNTs have the

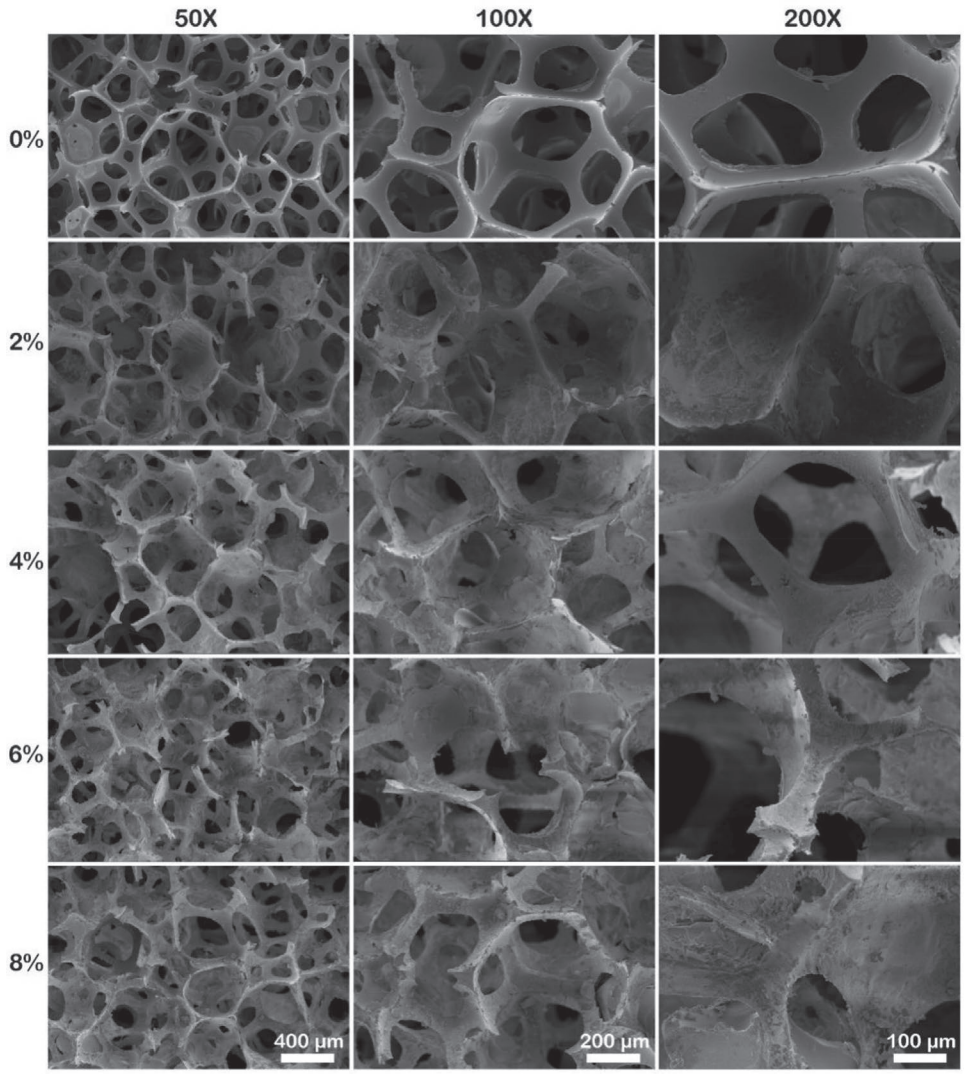

Figure 2. SEM images of PUF and HNTs-PUF in different magnifications.

element composition of oxygen (53.72%), aluminum (11.46%), and silicon (13.23%).[44] An increase in oxygen and aluminum content and a decrease in carbon content of the HNTs-PUF indicates that the nanotubes are successfully coated. The content of aluminum, silicon, oxygen of the modified foam increases from 0.3% to 12.33%, from 5.9% to 14.39%, from 24.49% to 55.84%, respectively. In contrast, the content of carbon and nitrogen decreases from 66.96% to 16.76% and from 2.54% to 0.69% after treatment. As shown in Figure 3C, the high-resolution spectra of XPS also indicate adhesion of HNT coating on the PUF, in which the peak intensities of Al2p and Si2p increase. The content of nitrogen on the modified PUF is very low, which indicates that HNTs are almost completely coated with surfaces of PUF. However, the high-resolution spectrum of PUF also has a Si2p photoelectron peak. The possible reason is that PUF has been modified by silicon-containing compound (silane) during fabrication. PU modified by the silicon material can improve the heat and water resistance of material.[45,46]

The composition of HNTs-PUF was investigated by energy dispersive spectrometer (EDS). The element mapping of O, Si, and Al is shown in **Figure 4**. The images were obtained through scanning the area in the first image of Figure 4. Consistent with the previously obtained SEM image results, the main components of HNTs (Si and Al) are densely distributed on the PUF skeleton. The results of EDS spectra are consistent with SEM and XPS results, which confirms that HNTs are successfully and uniformly decorated on the PUF skeleton.

The HNTs-PUF was further characterized by X-ray diffraction (XRD) and fourier transform infrared spectroscopy (FTIR). The XRD patterns for HNTs and all the PUF samples were presented in **Figure 5**A. The raw HNTs show diffraction reflection at $2\theta = 11.7°$, 20.1°, 24.7°, and 35° assigned to (001), (020, 1 0), (002), (200, 130) plane, respectively. The peaks around 18° and 30° in the HNT pattern are attributed to the impurities of alum and quartz.[44] For raw PU, an amorphous diffraction peak is seen around $2\theta = 21°$. Due to the presence of hydrogen bonds interactions in hard segment of the PU, the degree of crystallinity is generally related to the ordered structure of the segments.[47] HNTs-PUF exhibits the same diffraction peak as the uncoated PUF diffraction peak

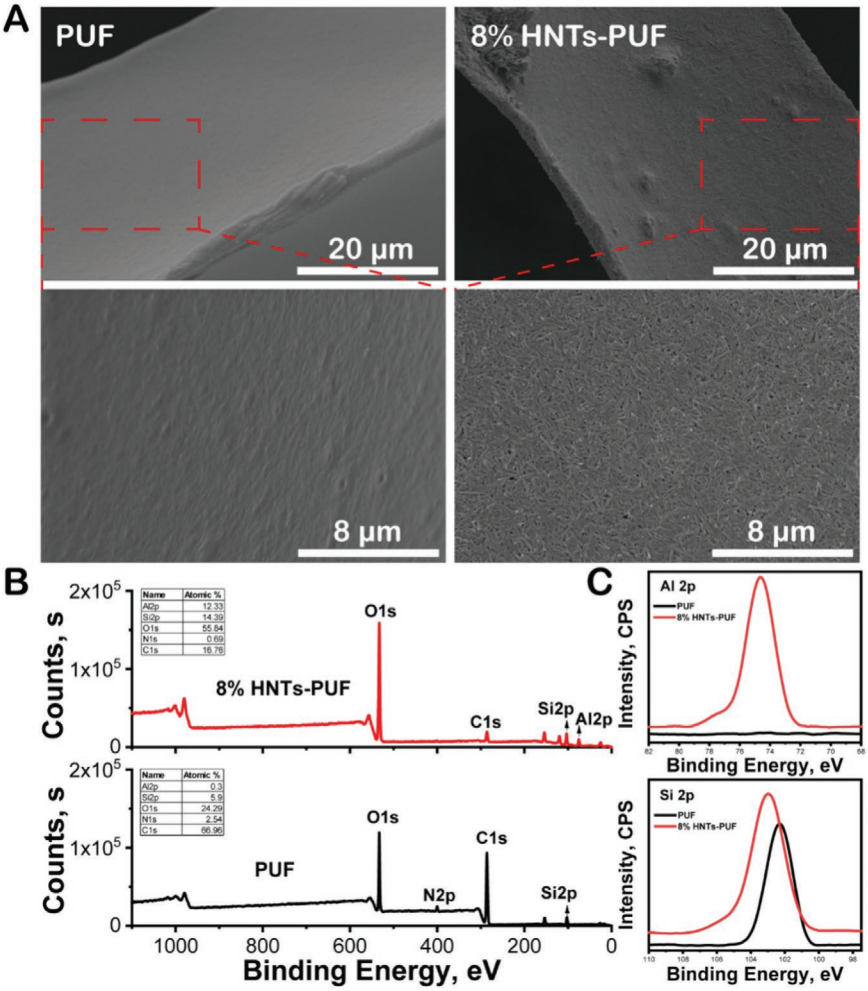

Figure 3. A) SEM images of PUF and 8% HNTs-PUF surface. B,C) XPS spectra of PUF and 8% HNTs-PUF.

at $2\theta = 21°$, but the peak shape change and the peak become sharper. In addition, the diffraction peak of PUF after decoration of HNTs is slightly shifted from the peak of raw HNTs. This may be due to the fact that HNTs bind to the PUF surface through physical interactions. The FTIR spectra for HNTs and all the PUF samples were presented in Figure 5B. The peaks of HNTs (3695 and 3622 cm^{-1}) appear in the FTIR spectrum (Figure 5B), which is attributed to the O—H stretching of inner-surface hydroxyl groups and O—H stretching of inner hydroxyl groups respectively.[48] The peak intensities of these two bands increase with the increase of HNT content. The peak around 1030 cm^{-1} is attributed to the asymmetrical stretch vibration absorption of Si—O—Si and a single Al—OH bending band is located at 910 cm^{-1}.[49] For uncoated PU, the peak around 1080 cm^{-1} is attributed to the irregular stretching vibration of C—O—C. The peaks at this position of the HNTs-PUF are shifted at different levels, which is attributed to the formation of hydrogen bonding interactions between HNTs and PU. From the FTIR results, it also can be found that the HNT coating can be uniformly bonded to the PUF surface by physical interactions.

2.3. Properties of HNTs-PUF

Figure 6A compares the density, porosity, and load capacity of HNTs-PUF. Uncoated PUF has the lowest density of 25.5 mg cm^{-3}. The density of PUF after coating HNTs is higher than that of uncoated PUF and increased with the increases of the HNT concentration. The increase in density of HNTs-PUF is attributed to more HNTs in the same volume. The increased density can bring the increase in the compressive strength of the PUF, which will be illustrated below. The porosity of PUF decreases slightly with the increase of HNT content, but the PUF coated with 8% concentration of HNTs also has a porosity of more than 60%. The porosity also affected the mechanical properties of the foams. Generally, a decrease in porosity resulted in a more compact structure, resulting in an increase in the mechanical strength of the porous material. So, the reduction in the porosity may also be a reason for increased mechanical strength. As expected, the compressive properties of the HNTs-PUF are significantly increased by incorporation of HNTs (Figure 6B). For example, the compressive strength at 60% strain of 8% HNTs-PUF is 21 kPa which is sevenfold that of PUF. After introduction of HNTs, the stiffness of the PUF is increased and the flexibility of the foam may be reduced due to the rigid character of the inorganic tubes. Previous studies also demonstrate that the addition of HNTs can improve the compressive properties of polymer scaffold effectively.[33,50,51] However, the mechanical strength of foam may still be improved, and better mechanical strength is needed in practical applications.

The thermal decomposition stability of the different foams was compared by thermogravimetric analysis (Figure 6). Raw HNTs show 16.9% weight loss from 50 to 700 °C, which is mainly attributed to the loss of adsorbed water and hydroxyl dehydration. After the introduction of HNT coating, thermal stability of PUF is improved. Uncoated PUF undergoes two stages of non-oxidative thermal degradation. In the initial stage, the initial degradation temperature is about 250 °C and the peak temperature is about 291 °C, which are attributed to the depolymerization of PU hard segment into isocyanate units. The polyol then degrade with an onset temperature of about 355 °C which is related to the formation of a molten pool and rapid mass loss.[38] After 450 °C, PUF is almost completely degraded, leaving only HNTs. The hydroxyl condensation of HNTs to form water further absorbes heat around 500 °C, thereby improving the thermal stability of the material. Uncoated PUF is almost completely decomposed in the temperature range of 350–450 °C, and the residue at 700 °C is 0.67%.

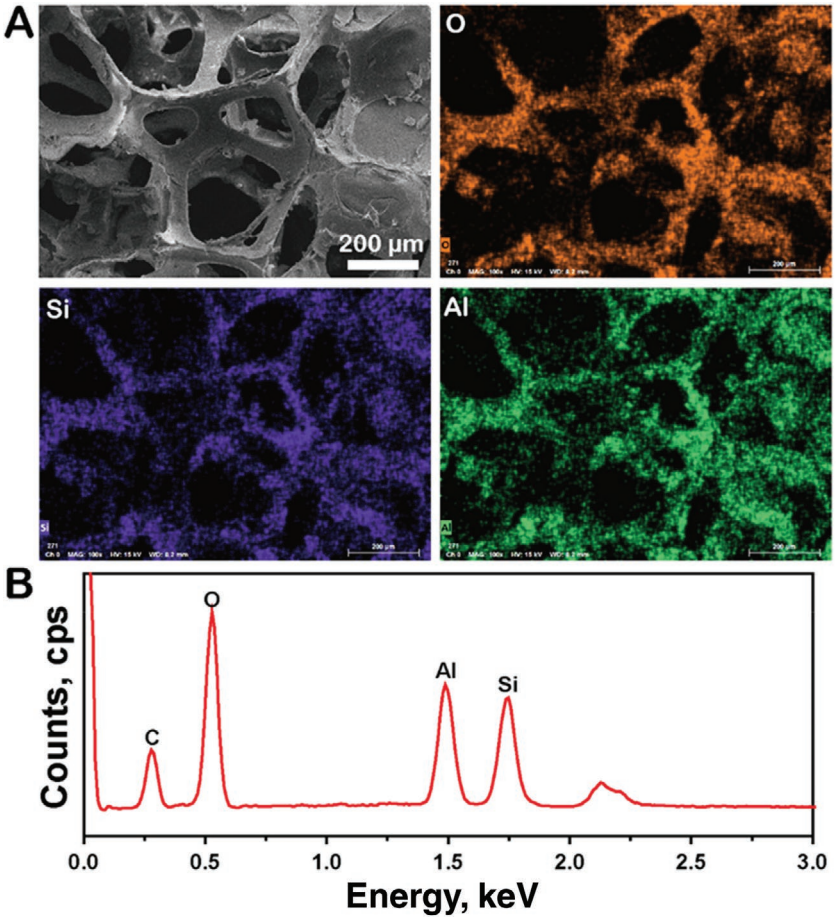

Figure 4. A) SEM images and the corresponding EDS mapping. B) EDS spectrum of the HNTs-PUF.

In contrast, when HNTs are coated on PUF, the remaining weight of the composite of 2%, 4%, 6%, 8% HNTs at 700 °C is 15.37%, 33.47%, 42.79%, 54.14%, respectively. The content of HNTs coated on PUF is 19.21%, 40.32%, 51.55%, 65.23% calculated from the TGA results, respectively. At the low concentration (2%), the initial degradation temperature and the second degradation temperature increase, but at high concentrations, the initial degradation temperature and the second degradation temperature decrease. Therefore, HNTs may have two opposite effects on the thermal degradation of PU, that is, HNTs slightly hinder the degradation of PU at low content, while HNTs accelerate the degradation of PU for 4%, 6%, and 8% of the samples. The accelerated degradation behavior of polymers by nanoclay has also been found in other systems, which is attributed to chromophoric groups and/or traces of iron in HNTs.[52,53] The decomposition temperature around 500 °C of HNTs-PUF decreases as the increase in the HNT concentration. This peak is related to the dehydration of the hydroxyl groups on the surface of the nanotubes.[25] The decrease may be due to the dehydration of the PU degradation product and HNTs.

The surface water contact angle reflects the hydrophilicity, which will affect the moisture absorption and permeability of the material. Super-hydrophilic materials show potentials as oil–water separation devices.[54] After HNT coating, the hydrophilicity of PUF is greatly improved (**Figure 7**A,G), and the water contact angle is changed from 116° to 0° because of the hydroxyl groups on the surfaces of HNTs. In contrast, the hydrophobic groups are located on the surface of PUF (alkyl and ester groups). As shown in Figure 7, the uncoated PUF does not exhibit super-hydrophilicity under oil, and they cannot pick up the methylene blue (MB) dyed water. Super-hydrophilicity of the HNTs-PUF makes them capable of adsorbing water completely from the oil phase very quickly. The test video for water absorption is provided in Video S1, Supporting Information.

PUF is one kind of adsorption materials which can effectively remove dyes, metal ions, and other toxicants from the sewage.[55,56] PUF composite shows increased adsorption ability compared with raw foam.[57,58] To investigate the dye adsorption ability of PUF, PUF (0.5 g) was immersed in an aqueous solution of MB (3.75×10^{-3} g L^{-1}, 20 mL) for a period of time. The UV–vis absorption spectra of the test solutions at different times were used to estimate the adsorption process (**Figure 8**). The result shows that the color of the HNTs-PUF treated MB solution become lighter with time, while the color of the MB solution adsorbed by raw PUF does not change significantly (Figure 8A). Consistent with the appearance observed by naked eye, HNTs-PUF has a strong adsorption capacity toward MB from the UV curves. The typical MB absorption band disappears after adsorption, and the MB solution after centrifugation is totally clear and transparent. Compared with uncoated PUF, the adsorption capacity of HNTs-PUF increases from 0.02 to 0.15 mg g^{-1}, and the adsorption efficiency

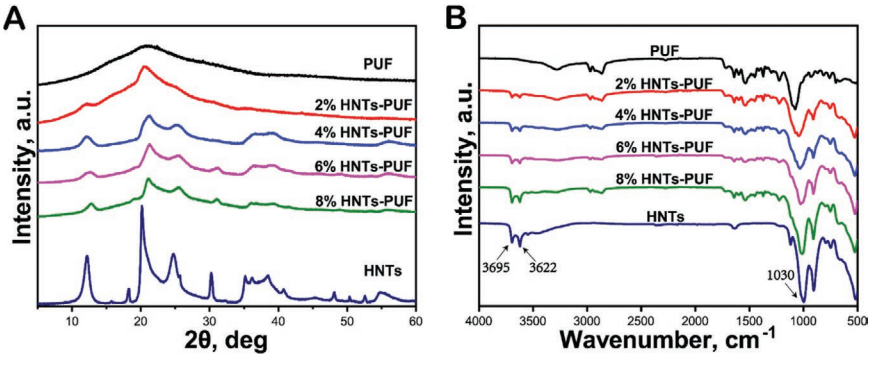

Figure 5. A) XRD patterns and B) FTIR spectra of HNTs, PUF, and HNTs-PUF.

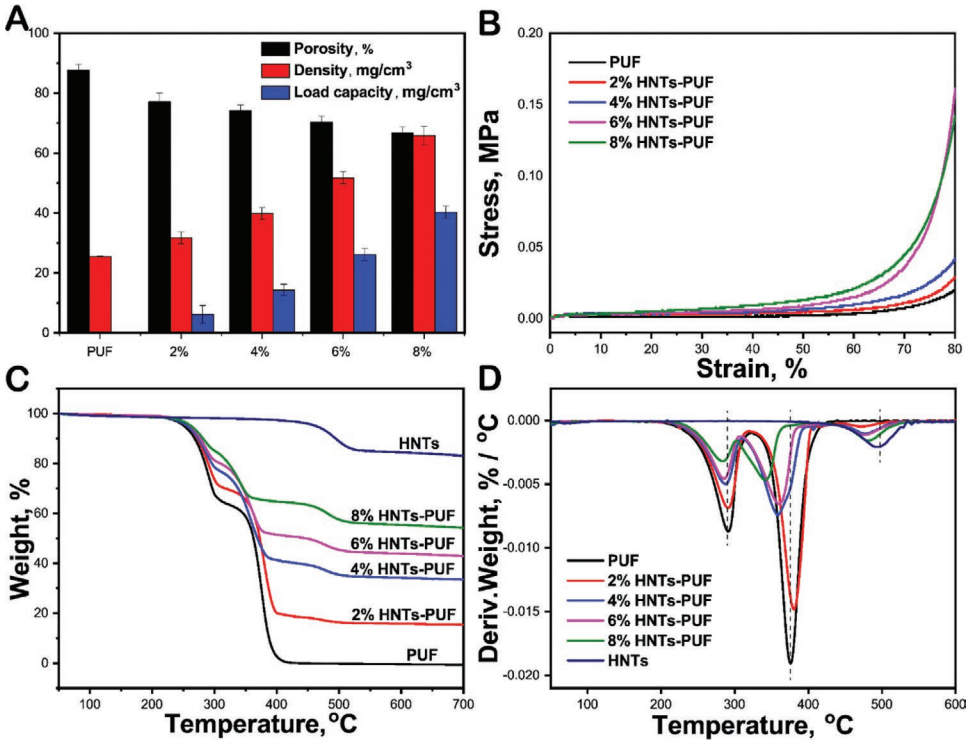

Figure 6. A) The porosity, density, and load capacity of PUF and HNTs-PUF. B) The compressive stress–strain curve of raw material and HNTs-PUF. C) Weight loss and D) derivative weight as a function of temperature for raw material and HNTs-PUF.

increases from 14% to 98% in 10 s. This is because HNTs have tubular structure with high surface areas, which is critical for the improvement of the dye adsorption performance.[59] Adsorption ability of HNTs-PUF is universal since HNTs are capable of adsorbing dyes and metal ions. For example, HNTs are capable of adsorbing dyes such as Rhodamine B, methylene blue, methyl violet, methyl orange, and neutral red in aqueous solution.[60–63] The HNTs-PUF has a high porosity, which is also a key factor to possess the high adsorption ability to MB in an aqueous solution. This suggests that HNTs-PUF may be used in wastewater treatment applications, showing potential value for environmental-restoration. The stability of HNT coatings in water needs to be further improved since they were easily dispersed in water and then deposited at the bottom of the beaker. Although there are hydrogen bonding interactions between HNTs and PU, the adhesion and durability of the HNT coating on PUF also need to be improved, since part of the coating may peel off when pressed by a large external force. However, modification of HNTs by dopamine and then coating them can form a layer of polydopamine (PDA) film which could firmly adhere to the PUF surfaces (Figure S4, Supporting Information).

The PUF samples were subjected to an open flame test to evaluate the flame retardancy of the modified PUF. The PUF sample was exposed to a butane torch for 10 s and then monitored until the flame was extinguished (**Figure 9**). Uncoated PUF is rapidly ignited, producing smoke and fumes when exposed to the torch. Meanwhile, the melting and dripping take place, potentially igniting flammable materials such as carpets and textiles (Video S2, Supporting Information). However, the HNTs-PUF can be automatically extinguished, and the flame retardancy performance is better with the increased of HNT concentration. In addition, the addition of HNT coating reduces smoke and dust emissions, while also prevent the production of oil droplets that can ignite other flammable materials (Video S3, Supporting Information). HNT coating can interrupt the thermal

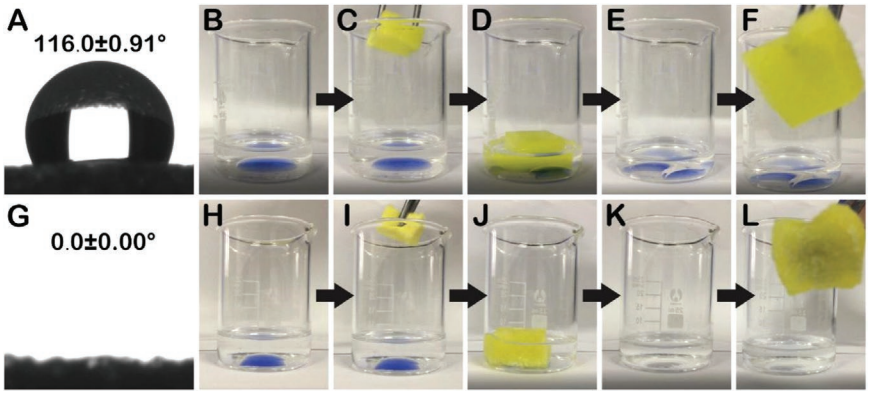

Figure 7. A,G) Contact angle image of PUF and HNTs-PUF. B–F) Chronological images of PUF and H–L) HNTs-PUF picking up water from a petroleum ether/water mixture. Water has been dyed with blue color for easier visualization.

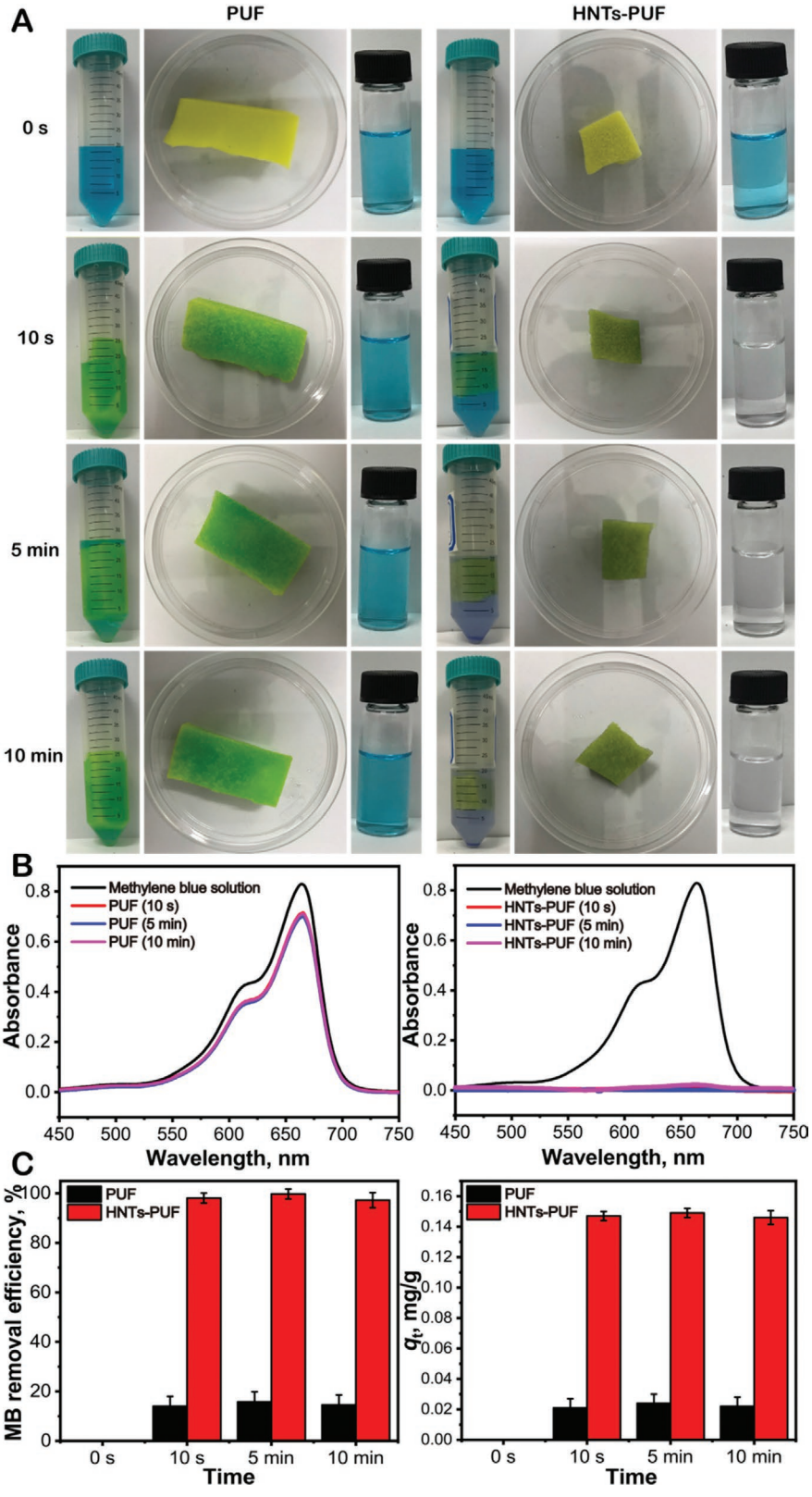

Figure 8. A) Adsorption ability of PUF and HNTs-PUF. B) UV–vis spectra of the original MB solution and those after treatment with PUF and HNTs-PUF at different time. C) Adsorption capacity and adsorption efficiency of PUF and HNTs-PUF.

degradation of the PUF by providing an insulating shield and prevent flammable degradation materials from spilling into the flame zone. The flame eventually gets extinguished because there is no fuel that can be burned.[25] The aluminum-containing hydroxide of HNTs can release water at high temperature, which is an endothermic process that releases water vapor to dilute the combustible gas and suppresses the release of toxic fumes, thereby increasing the flame retardancy of PUF.[64]

In order to study the flame retardancy in more details, the samples were tested in an limited oxygen index (LOI) tester according to the standard protocol (GB/T 2406, China). LOI is a test method commonly used to evaluate the flammability of materials. It is defined as the minimum fraction of oxygen in the O_2/N_2 atmosphere mixture required for material combustion and is the quantitative standard for determining the flame-retardant properties of materials.[65] The results in **Table 1** show that coatings with different concentrations of HNTs have a certain effect on the LOI results of PUF. It can be seen that the LOI value of the PUF sample is the lowest, only 19. However, the LOI values for the 4% and 6% HNTs-PUF are greater than 21, which means that PUF coated with HNTs is more fire-resistant than uncoated PUF. The barrier effect of HNTs layer is considered as the main cause of the increase in LOI value. The burning rates of PUF and HNTs-PUFs are determined by horizontal burning test. The results showed that 6% and 8% HNTs-PUF have good flame-retardant properties and they cannot be ignited. However, as the concentration of HNTs increases from 2% to 4%, the burning rate of PUF increases. This may be because the HNTs coating can form a protective layer to prevent flame spread, thereby preventing PUF from melting into molten droplets, and most of the heat is not taken away. Therefore, the process of thermal feedback to the PUF cannot be interrupted, eventually resulting in a faster burning rate. In summary, from the flame retardance testing result, the concentration for PUF coating of HNTs suspension should be more than 6%.

The combustion residues of PUF and HNTs-PUF were dissolved in ethanol

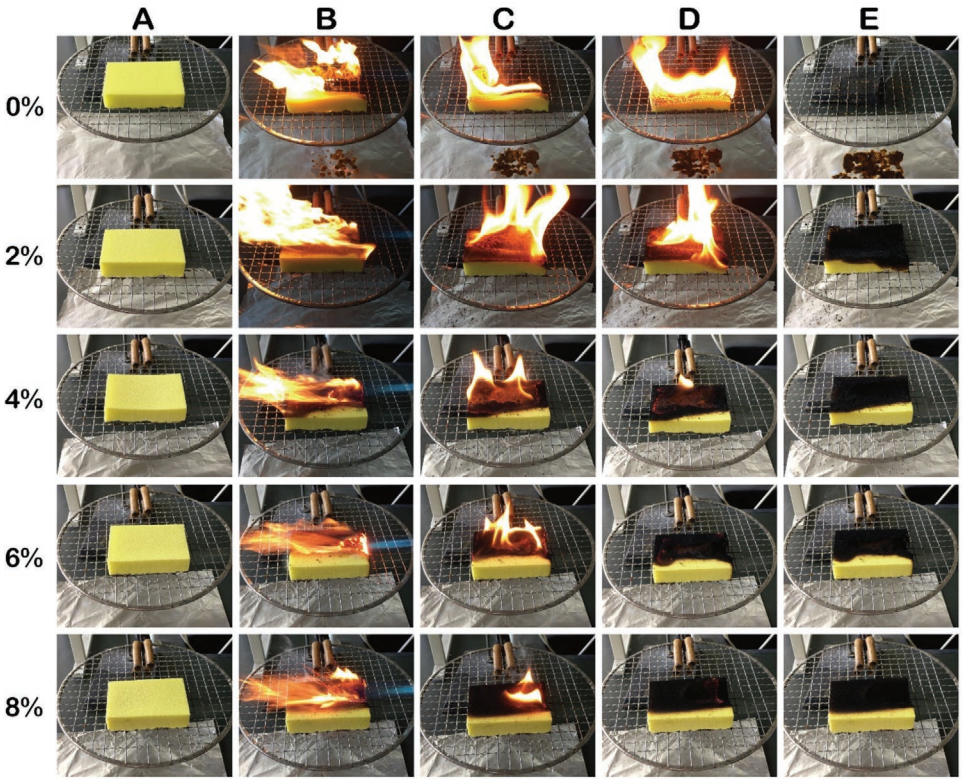

Figure 9. Torch burn test images of PUF and HNTs-PUF. A) Before exposure to the torch flame; B) after exposure to the torch flame for 5 s; C) remove the torch flame; D) remove the torch flame for 5 s; E) auto-extinguish.

absolute and further analyzed by TEM and SEM (Figure S5, Supporting Information). The results show that the PUF only has melted oil after burning, while the main products of HNTs-PUF after combustion are mainly tubular HNTs. It also can be seen that the tubular structure of HNTs is not destroyed, and the PUF melt can wrap the tubes to form an isolation layer to isolate the fire source and oxygen. It is verified again that HNTs improve the flame retardancy of PUF by the mechanism of thermal insulation and char reinforcement of the HNT coating.

3. Conclusion

In summary, significantly improved flame retardance and dye adsorption property of PUF were prepared by facile dip-coating of the cheap and environmental-friendly HNTs. The results of SEM, POM, XPS, XRD, and FTIR show that the HNT coating can be uniformly assembled to the PUF surfaces. The coated PUF maintains high porosity and mechanical properties with improved hydrophilicity, adsorption properties, and flame retardancy. The MB adsorption capacity of HNTs-PUF increases from 0.02 to 0.15 mg g^{-1} compared with PUF, and the dye removal efficiency reaches 98% at 10 s. In the torch burning test, the HNT coating maintains a large degree of PUF surface with a high degree of integrity, which prevents melt from igniting other flammable materials. The modification of the foam is easy to scale up because it does not use complex processes or sophisticated equipment. The concept and technique can be extended to other polymer materials, such as fibers and bulk materials. HNT-coated polymers show great potential in functional materials such as flame-retardant materials and environmental-restoration materials.

Table 1. The influence of HNTs concentration on the retardancy of the PUF.

Sample	Limiting oxygen index [%]	Dripping drops	Burn to 25 mm	Burning rate [mm min^{-1}]
0%	19	Yes	Yes	300.6
2%	20	No	Yes	500.0
4%	21	No	Yes	470.3
6%	23	No	No	–
8%	23	No	No	–

4. Experimental Section

Materials and Reagents: High-purity halloysite (white, powder) was purchased from Guangzhou Runwo Materials Technology Co. Ltd., China. PUF with open-cell structure was purchased from 3M Co. Ltd., China. Ethanol absolute (density of 0.790 g mL^{-1} (20 °C)) was purchased from Tianjin Baishi Chemical Co. Ltd., China. All of the other chemicals were of analytical reagent grade and were used without further purification. Ultrapure water was purified by deionization and filtration with a Millipore purification apparatus (resistivity > 18.2 MΩ·cm).

Preparation of HNT Suspension: In order to study the effect of HNTs on the flame retardancy of PUF, different HNT suspensions were prepared. In a typical procedure, 2, 4, 6, and 8 g HNTs were dispersed via ultrasonication (40 kHz) in 100 mL of ultrapure water for 30 min.

Preparation of HNTs Dip-Coated PUF: The preparing process of HNTs-PUF by dip-coating methods is shown in Figure 1A. First, the commercial PUF was washed successively with ultrapure water using an ultrasonic cleaner (SK1200H, Shanghai Kedao Ultrasonic Instrument Co. Ltd., China), and then dried in a vacuum oven (DZF-6051, Shanghai Yiheng Scientific Instrument Co. Ltd., China) at 100 °C for several hours to completely remove moisture. The dried PUF was then dipped into the suspension of HNTs in ultrapure water and repeatedly squeezed until no bubbles were produced. Finally, it was dried in the vacuum oven at 100 °C for 2 h. During the drying process of HNTs-PUF, HNTs may be unevenly coated due to the influence of gravity. Increasing the temperature would shorten the drying time which was beneficial for the distribution of the HNTs inside the foam. One should turn over the PUF surface every half an hour to make sure the HNT coating uniform.

Characterization: ξ-Potential Analysis: Zeta potential of HNTs aqueous dispersion was tested using a multi-angle particle size and high sensitivity Zeta potential analyzer (NanoBrook Omni, Brookhaven Instruments Ltd., USA) at 25 °C. The dispersion was tested at pH of 7.8.

Dynamic Light Scattering (DLS): The size of HNTs in aqueous dispersion (0.05 wt.%) was tested by a multi-angle particle size and high sensitivity Zeta potential analyzer (NanoBrook Omni, Brookhaven Instruments Ltd., USA) at 25 °C.

Polarized Optical Microscope (POM): Sectioned PUF and HNTs-PUF with thickness of 1 mm were placed on a glass sheet, and then the photographs were taken by using POM (BX51, Olympus Corporation, Japan).

Field Emission Scanning Electron Microscope (FE-SEM): The geometric morphologies of PUF and HNTs-PUF before and after the torch burn testing were observed by a FE-SEM (ULTRA55, Carl Zeiss Jena Co. Ltd., Germany) at 5 kV. Before FE-SEM observation, the samples were sputter-coated with gold films with a thickness of 5 nm.

X-ray Photoelectron Spectrum (XPS): The X-ray photoelectron spectroscopy analysis of PUF and HNTs-PUF were analyzed by XPS instrument (ESCALAB250Xi, Thermo Fisher Scientific Co. Ltd., USA). The atoms of N, C, O, Al, and Si were detected.

Energy Dispersive Spectrometer (EDS): The chemical composition of the sample was determined by EDS at 15 kV, which was an attachment to FE-SEM.

Fourier Transform Infrared Spectroscopy (FTIR): The FTIR spectra of PUF and HNTs-PUF were measured using attenuated total reflectance (ATR) using a Thermo FTIR (Nicolet iS50, Thermo Fisher Scientific Co. Ltd., USA). The scans were performed 32 times in succession and their average values were saved. The spectra were taken from 4000 to 500 cm^{-1}. The wavenumber resolution was 2 cm^{-1}.

X-ray Diffraction (XRD): The XRD patterns were obtained using XRD machine (Miniflex600, Rigaku Corporation, Japan) at an accelerating voltage of 40 kV with current of 40 mA.

Density: The density of the samples was determined by measuring weight and volume of each individual foam. The weight of the samples was measured by an analytical balance (readable 0.0001 g, ME204E, METTLER TOLEDO Co. Ltd., Switzerland), and the size of the samples was measured by a digital caliper. Five samples were used for density determination for each group. The density was calculated by the following equation.

$$\text{density} = \frac{m}{lwh} \tag{1}$$

where m, l, w, and h are the mass, length, width, and height of the samples, respectively.

Porosity: The porosity of the samples was measured by the following procedure. First, the size and weight of the samples were measured and recorded, respectively. The samples of different HNT contents were then immersed in ethanol absolute for 24 h at room temperature. Finally, the samples were gently taken and weighed. Five samples were used for porosity determination for each group. The porosity was calculated by the following equation.

$$\text{porosity} = \frac{m_a - m}{\rho lwh} \times 100\% \tag{2}$$

where m_a is the weight of the samples after soaking in ethanol absolute. ρ is the density of ethanol absolute. m, l, w, and h are the mass, length, width, and height of the samples before soaking in ethanol absolute, respectively.

Load Capacity: The load capacity of HNTs on PUF composite was determined by measuring the weight of the foam before and after coating of HNTs, which was calculated by the following equation.

$$\text{load capacity} = \frac{m - m_o}{V} \tag{3}$$

where V is the volume of the foam. m_o and m are weight of the foam before and after loading of HNTs, respectively.

Mechanical Property Test: The compressive stress–strain curves were measured using a universal testing machine (UTM-Q422, Chengde Jinjian Testing Instrument Co. Ltd, China), and the compressive rate was 10 mm min^{-1}. The samples used for the test were a cuboid sample with the side length of 10 mm.

Thermo Gravimetric Analyzer (TGA): The TGA curves were tested using the TGA (TGA2, METTLER TOLEDO Co. Ltd., Switzerland) under a nitrogen atmosphere from 50 to 700 °C at a heating rate of 10 °C min^{-1}.

Water Contact Angle (WCA): The surface hydrophilicity was determined using a drop-shape analyzer (DSA100, Kruss Co. Ltd., Germany) at room temperature. The contact angle was measured just after the liquid deposition onto the substrate. The liquid droplet volume was 5.0 ± 0.5 µL. Five measurements at least were carried out on each sample.

Adsorption Measurements: The adsorption experiment was carried out with PUF (0.5 g) as a sorbent of MB solution (3.75×10^{-3} g L^{-1}, 20 mL) in a centrifuge tube at room temperature. After the absorption experiment, PUF was separated from the mixture using centrifugation. Measurement of MB solution concentration by UV–vis spectrophotometer (UV-2550, Shimadzu Instrument Co., Ltd., China) at 450–750 nm. The adsorption capacity and removal efficiency were calculated according to the following relations.

$$q_t = \frac{(c_o - c_t)V}{m} \tag{4}$$

$$\text{removal efficiency} = \frac{c_o - c_t}{c_o} \times 100\% \tag{5}$$

where q_t represents the adsorption capacity at time t, c_o, and c_t represent the concentration of MB solution before and after being adsorbed for a certain time (t), respectively. m and V represent the mass of the foam and the volume of MB solution, respectively.

Torch Burn Test: Foam flammability was qualitatively evaluated by exposure to direct flame from a butane torch for 10 s. A blue flame from a butane torch implied that the flame temperature was approximately 1300 °C. The burning behaviors of samples (e.g., flame spread, dripping, charring, and receding away from flame) were evaluated visually and videos were recorded. To ascertain the flammability of the material, observations from the test were analyzed in correlation with combustion tests.

Limiting Oxygen Index (LOI): Fire property of foam samples was performed according to GB/T 2406 using by oxygen index tester (HC-2C, Nanjing Shang Yuan Analytical Instrument Co., Ltd., China). In the LOI test, all samples were placed in a vertical glass column using a sample holder, and adjusted gas flow (oxygen and nitrogen) to confirm the standard test technique. Each sample was ignited with a flame and was burned downward into the unheated material. Then, minimum oxygen concentrations supporting combustion for all samples were recorded as a percentage.

Horizontal Burning Test: The burning rate of the horizontal combustion was measured by a horizontal vertical flame tester (YH-8920US, Yue Hua

Electric Industrial Co. Ltd., China). The sample was held horizontally and a flame was applied to one end of the sample. The time for the flame to reach from the first reference mark (25 mm from the end) to the second reference mark, which was at 100 mm from the end, was recorded. Three measurements at least were carried out on each sample. Then, burning rates of the composites were calculated as follows.

$$V = 60\,L/t \quad (6)$$

where V is the burning rates, L is the burned length, and t is the time of burning.

Transmission Electron Microscopy (TEM): The morphologies of samples were observed by TEM (JEM-2100F, JEOL Co. Ltd., Japan) under an accelerating voltage of 100 kV. The samples were ultrasonically dispersed in ethanol absolute or ultrapure water and dropped on the copper network before observation.

Supporting Information

Supporting Information is available from the Wiley Online Library or from the author.

Acknowledgements

This work was financially supported by National Natural Science Foundation of China (51473069 and 51502113) and Pearl River S&T Nova Program of Guangzhou (201610010026).

Conflict of Interest

The authors declare no conflict of interest.

Keywords

absorbency, dip-coating, flame retardancy, halloysite nanotubes, polyurethane foams

Received: April 11, 2019
Revised: May 31, 2019
Published online: June 25, 2019

[1] C. Boujard, N. Foray, J. Caudron, *Report 1202C0079, ADEME* **2014**.
[2] K. M. Zia, H. N. Bhatti, I. A. Bhatti, *React. Funct. Polym.* **2007**, *67*, 675.
[3] H. Pan, Y. Lu, L. Song, X. Zhang, Y. Hu, *Compos. Sci. Technol.* **2016**, *129*, 116.
[4] D. Patra, P. Vangal, A. A. Cain, C. Cho, O. Regev, J. C. Grunlan, *ACS Appl. Mater. Interfaces* **2014**, *6*, 16903.
[5] G. Laufer, C. Kirkland, A. B. Morgan, J. C. Grunlan, *ACS Macro Lett.* **2013**, *2*, 361.
[6] R. Davis, Y.-C. Li, M. Gervasio, J. Luu, Y. S. Kim, *ACS Appl. Mater. Interfaces* **2015**, *7*, 6082.
[7] H. Kim, D. W. Kim, V. Vasagar, H. Ha, S. Nazarenko, C. J. Ellison, *Adv. Funct. Mater.* **2018**, *28*, 1803172.
[8] J. Lefebvre, B. Bastin, M. Le Bras, S. Duquesne, R. Paleja, R. Delobel, *Polym. Degrad. Stab.* **2005**, *88*, 28.
[9] M.-J. Chen, Z.-B. Shao, X.-L. Wang, L. Chen, Y.-Z. Wang, *Ind. Eng. Chem. Res.* **2012**, *51*, 9769.
[10] Y. Pan, J. Zhan, H. Pan, W. Wang, G. Tang, L. Song, Y. Hu, *ACS Sustainable Chem. Eng.* **2016**, *4*, 1431.
[11] W.-H. Rao, Z.-M. Zhu, S.-X. Wang, T. Wang, Y. Tan, W. Liao, H.-B. Zhao, Y.-Z. Wang, *Polym. Degrad. Stab.* **2018**, *153*, 192.
[12] H. Xie, W. Yang, A. C. Y. Yuen, C. Xie, J. Xie, H. Lu, G. H. Yeoh, *Chem. Eng. J.* **2017**, *311*, 310.
[13] B. Zhang, H. Liu, J. Han, *J. Phys. Chem. Solids* **2018**, *115*, 199.
[14] S. Gaan, S. Liang, H. Mispreuve, H. Perler, R. Naescher, M. Neisius, *Polym. Degrad. Stab.* **2015**, *113*, 180.
[15] A. Dasari, Z.-Z. Yu, G.-P. Cai, Y.-W. Mai, *Prog. Polym. Sci.* **2013**, *38*, 1357.
[16] Z.-J. Cao, X. Dong, T. Fu, S.-B. Deng, W. Liao, Y.-Z. Wang, *Polym. Degrad. Stab.* **2017**, *136*, 103.
[17] M. Thirumal, D. Khastgir, G. Nando, Y. Naik, N. K. Singha, *Polym. Degrad. Stab.* **2010**, *95*, 1138.
[18] H. Pan, L. Song, L. Ma, Y. Pan, K. M. Liew, Y. Hu, *Cellulose* **2014**, *21*, 2995.
[19] X. Wang, Y. T. Pan, J. T. Wan, D. Y. Wang, *RSC Adv.* **2014**, *4*, 46164.
[20] F. Carosio, C. Negrell-Guirao, J. Alongi, G. David, G. Camino, *Eur. Polym. J.* **2015**, *70*, 94.
[21] Q. Wu, Q. Zhang, L. Zhao, S.-N. Li, L.-B. Wu, J.-X. Jiang, L.-C. Tang, *J. Hazard. Mater.* **2017**, *336*, 222.
[22] F. Ding, J. Liu, S. Zeng, Y. Xia, K. M. Wells, M.-P. Nieh, L. Sun, *Sci. Adv.* **2017**, *3*, e1701212.
[23] G. Laufer, C. Kirkland, A. A. Cain, J. C. Grunlan, *ACS Appl. Mater. Interfaces* **2012**, *4*, 1643.
[24] K. M. Holder, A. A. Cain, M. G. Plummer, B. E. Stevens, P. K. Odenborg, A. B. Morgan, J. C. Grunlan, *Macromol. Mater. Eng.* **2016**, *301*, 665.
[25] K. M. Holder, R. J. Smith, J. C. Grunlan, *J. Mater. Sci.* **2017**, *52*, 12923.
[26] H. Pan, Y. Pan, W. Wang, L. Song, Y. Hu, K. M. Liew, *Ind. Eng. Chem. Res.* **2014**, *53*, 14315.
[27] D. D. Nguyen, N.-H. Tai, S.-B. Lee, W.-S. Kuo, *Energy Environ. Sci.* **2012**, *5*, 7908.
[28] Y. Liu, J. Ma, T. Wu, X. Wang, G. Huang, Y. Liu, H. Qiu, Y. Li, W. Wang, J. Gao, *ACS Appl. Mater. Interfaces* **2013**, *5*, 10018.
[29] M. Liu, Z. Jia, D. Jia, C. Zhou, *Prog. Polym. Sci.* **2014**, *39*, 1498.
[30] Y. M. Lvov, D. G. Shchukin, H. Möhwald, R. R. Price, *ACS Nano* **2008**, *2*, 814.
[31] E. Joussein, S. Petit, J. Churchman, B. Theng, D. Righi, B. Delvaux, *Clay Miner* **2005**, *40*, 383.
[32] M. Liu, B. Guo, M. Du, X. Cai, D. Jia, *Nanotechnology* **2007**, *18*, 455703.
[33] M. Liu, C. Wu, Y. Jiao, S. Xiong, C. Zhou, *J. Mater. Chem. B* **2013**, *1*, 2078.
[34] F. Wu, J. Zheng, Z. Li, M. Liu, *Chem. Eng. J.* **2019**, *359*, 672.
[35] D. C. O. Marney, L. J. Russell, D. Y. Wu, T. Nguyen, D. Cramm, N. Rigopoulos, N. Wright, M. Greaves, *Polym. Degrad. Stab.* **2008**, *93*, 1971.
[36] H. Vahabi, M. R. Saeb, K. Formela, J.-M. L. Cuesta, *Prog. Org. Coat.* **2018**, *119*, 8.
[37] E. S. Goda, K. R. Yoon, S. H. El-sayed, S. E. Hong, *Thermochim. Acta* **2018**, *669*, 173.
[38] R. J. Smith, K. M. Holder, S. Ruiz, W. Hahn, Y. Song, Y. M. Lvov, J. C. Grunlan, *Adv. Funct. Mater.* **2018**, *28*, 1703289.
[39] G. Cavallaro, G. Lazzara, S. Milioto, G. Palmisano, F. Parisi, *J. Colloid Interface Sci.* **2014**, *417*, 66.
[40] M. Liu, B. Guo, M. Du, D. Jia, *Appl. Phys. A* **2007**, *88*, 391.
[41] Z. Luo, A. Wang, C. Wang, W. Qin, N. Zhao, H. Song, J. Gao, *J. Mater. Chem. A* **2014**, *2*, 7327.
[42] Z. Luo, H. Song, X. Feng, M. Run, H. Cui, L. Wu, J. Gao, Z. Wang, *Langmuir* **2013**, *29*, 12358.
[43] R. Jalili, S. H. Aboutalebi, D. Esrafilzadeh, K. Konstantinov, S. E. Moulton, J. M. Razal, G. G. Wallace, *ACS Nano* **2013**, *7*, 3981.

[44] K. Feng, G.-Y. Hung, J. Liu, M. Li, C. Zhou, M. Liu, *Chem. Eng. J.* **2018**, *331*, 744.
[45] P. Alves, J. F. J. Coelho, J. Haack, A. Rota, A. Bruinink, M. H. Gil, *Eur. Polym. J.* **2009**, *45*, 1412.
[46] L. F. Wang, Q. Ji, T. E. Glass, T. C. Ward, J. E. McGrath, M. Muggli, G. Burns, U. Sorathia, *Polymer* **2000**, *41*, 5083.
[47] L. Wang, Y. Shen, X. Lai, Z. Li, M. Liu, *J. Polym. Res.* **2011**, *18*, 469.
[48] M. Du, B. Guo, M. Liu, X. Cai, D. Jia, *Phys. B* **2010**, *405*, 655.
[49] H. Yu, Y. Zhang, X. Sun, J. Liu, H. Zhang, *Chem. Eng. J.* **2014**, *237*, 322.
[50] M. Liu, L. Dai, H. Shi, S. Xiong, C. Zhou, *Mater. Sci. Eng., C* **2015**, *49*, 700.
[51] B. Huang, M. Liu, C. Zhou, *Carbohydr. Polym.* **2017**, *175*, 689.
[52] S. Therias, M. Murariu, P. Dubois, *Polym. Degrad. Stab.* **2017**, *145*, 60.
[53] G. Gorrasi, V. Bugatti, M. Ussia, R. Mendichi, D. Zampino, C. Puglisi, S. C. Carroccio, *Polym. Degrad. Stab.* **2018**, *152*, 43.
[54] J. Yu, X. Zhao, Q. Zhao, G. Wang, *Mater. Chem. Phys.* **2001**, *68*, 253.
[55] S. Kumari, G. S. Chauhan, J. H. Ahn, *Chem. Eng. J.* **2016**, *304*, 728.
[56] S. H. Jang, B. G. Min, Y. G. Jeong, W. S. Lyoo, S. C. Lee, *J. Hazard. Mater.* **2008**, *152*, 1285.
[57] S. Ranote, D. Kumar, S. Kumari, R. Kumar, G. S. Chauhan, V. Joshi, *Chem. Eng. J.* **2019**, *361*, 1586.
[58] H.-J. Hong, J. S. Lim, J. Y. Hwang, M. Kim, H. S. Jeong, M. S. Park, *Carbohydr. Polym.* **2018**, *195*, 136.
[59] L. Yu, H. Wang, Y. Zhang, B. Zhang, J. Liu, *Environ. Sci.: Nano* **2016**, *3*, 28.
[60] P. Luo, Y. Zhao, B. Zhang, J. Liu, Y. Yang, J. Liu, *Water Res.* **2010**, *44*, 1489.
[61] R. Liu, B. Zhang, D. Mei, H. Zhang, J. Liu, *Desalination* **2011**, *268*, 111.
[62] Y. Xie, D. Qian, D. Wu, X. Ma, *Chem. Eng. J.* **2011**, *168*, 959.
[63] M. Massaro, C. G. Colletti, G. Lazzara, S. Guernelli, R. Noto, S. Riela, *ACS Sustainable Chem. Eng.* **2017**, *5*, 3346.
[64] T. Zheng, X. Ni, *RSC Adv.* **2016**, *6*, 57122.
[65] M. Sharifi, M. Ebrahimi, S. Jafarifard, *Prog. Org. Coat.* **2017**, *106*, 69.